

Neutrino-pair emission due to electron-phonon scattering in a neutron star crust

D.G. Yakovlev and A.D. Kaminker
Ioffe Physical-Technical Institute
194021, St.Petersburg, Russia

Abstract

Neutrino-pair bremsstrahlung radiation is considered due to electron-phonon scattering of degenerate, relativistic electrons in a lattice of spherical atomic nuclei in a neutron star crust. The neutrino energy generation rate is calculated taking into account exact spectrum of phonons, the Debye-Waller factor, and the nuclear form-factor in the density range from 10^7 g cm^{-3} to $10^{14} \text{ g cm}^{-3}$ at arbitrary nuclear composition for body-centered-cubic and face-centered-cubic Coulomb crystals. The results are fitted by a unified analytic expression. A comparison is given of the neutrino bremsstrahlung energy losses in a neutron star crust composed of ground state and accreted matter, in the solid and liquid phases.

1 Introduction

The neutrino-pair bremsstrahlung radiation of electrons in the liquid and crystalline phases of dense matter is one of the main cooling mechanisms of neutron star (NS) crusts. This radiation has been studied in a number of works (see, e.g., Itoh et al., 1989, and references therein). Recently Haensel et al. (1966) have reconsidered the neutrino radiation produced due to collisions of degenerate, relativistic electrons with atomic nuclei in the liquid phase, $e + (Z, A) \rightarrow e + (Z, A) + \nu + \bar{\nu}$. The authors have expressed the neutrino energy loss rate in a simple form through the Coulomb logarithm which depends weakly on the parameters of stellar matter. The Coulomb logarithm has been calculated and fitted analytically for matter with arbitrary nuclear composition at all densities and temperatures of practical interest. The proposed approach is invalid only in the deep layers of the NS crust ($\rho \sim 10^{14} \text{ g cm}^{-3}$), where the atomic nuclei can form clusters and/or have nonspherical shape (Lorenz et al., 1993, Pethick and Ravenhall, 1995).

In the present article, we also restrict ourselves to consideration of spherical atomic nuclei. We will study the neutrino-pair bremsstrahlung of electrons in the crystalline phase of dense matter. It is well known (e.g., Itoh et al., 1989) that this process has two channels. The first one is the neutrino radiation due to Bragg diffraction of electrons in a lattice (“the static lattice contribution”). The second one is the neutrino emission due to absorption or creation of phonons (“the phonon contribution”). It has been accepted until recently that both components have comparable intensities. However recently Pethick and Thorsson (1994) have shown that the band structure of crystals in a NS crust (the presence of an energy gap in the electron dispersion relation at the Brillouin zone boundaries) suppresses exponentially the static lattice contribution. Accordingly the phonon contribution dominates, and it will be the subject of our consideration.

The neutrino radiation due to the electron–phonon scattering has been studied earlier by Flowers (1973) and — in the frame of the Weinberg – Salam – Glashow theory — by Itoh et al. (1984a). The latter authors fitted their results by complicated analytic expressions and tabulated the fit parameters for matter with different nuclear compositions. These results are also included in the new review of Itoh et al. (1996). We will show that, in some cases, the fits of Itoh et al. (1984a, 1996) are not too accurate. We will carry out more accurate calculations and fit the results by a unified formula valid for matter with arbitrary nuclear composition. In addition to the body-centered-cubic crystals, which have been studied traditionally in the literature, we will consider also the face-centered-cubic crystals. For illustration, we analyse the neutrino–pair bremsstrahlung in the solid and liquid phases of NS crusts composed of ground–state or accreted matters.

2 Physical conditions

Consider matter of a NS crust in the density range $10^6 \text{ g cm}^{-3} \ll \rho \lesssim 10^{14} \text{ g cm}^{-3}$. In the domain of $10^6 \text{ g cm}^{-3} \ll \rho < \rho_{\text{ND}} \simeq 4 - 6 \times 10^{11} \text{ g cm}^{-3}$, which corresponds to the outer crust, the matter consists of atomic nuclei immersed in a nearly ideal relativistic and degenerate gas of electrons. In the inner crust, where $\rho > \rho_{\text{ND}}$, free neutrons appear in addition to the nuclei and electrons. If $\rho \gtrsim 10^{14} \text{ g cm}^{-3}$ the nuclei can be nonspherical and form clusters (Lorenz et al., 1993; Pethick and Ravenhall, 1995); the nuclei disappear at the bottom of the inner crust, at $\rho > 1.5 \times 10^{14} \text{ g cm}^{-3}$.

The state of degenerate electrons in the NS crust is characterized by the Fermi momentum p_{F} or the relativistic parameter x :

$$p_{\text{F}} = \hbar(3\pi^2 n_e)^{1/3}, \quad x = \frac{p_{\text{F}}}{m_e c} \approx 100.9 \left(\frac{\rho_{12}}{\mu_e} \right)^{1/3}, \quad (1)$$

where μ_e is the number of baryons per electron and ρ_{12} is density in units of $10^{12} \text{ g cm}^{-3}$. In the density range of study we have $\rho \gg 10^6 \text{ g cm}^{-3}$, and the electron gas is ultrarelativistic ($x \gg 1$). The electron degeneracy temperature is

$$T_{\text{F}} = T_0 (\sqrt{1 + x^2} - 1), \quad T_0 = \frac{m_e c^2}{k_{\text{B}}} \approx 5.930 \times 10^9 \text{ K}, \quad (2)$$

where k_{B} is the Boltzmann constant. We consider the case of $T \ll T_{\text{F}}$.

The state of nuclei (ions) is characterized by the ion–coupling parameter $\Gamma = Z^2 e^2 / (a k_{\text{B}} T) \approx 0.225 x Z^{5/3} / T_8$, where Ze is the nuclear charge, $a = [3 / (4\pi n_i)]^{1/3}$ is the mean inter–ion distance, n_i is the number density of nuclei, and T_8 is temperature in units of 10^8 K . At high enough temperatures, when $\Gamma \ll 1$, the nuclei constitute the Boltzmann gas. For lower T ($\Gamma \gtrsim 1$), the gas transforms into the Coulomb liquid, and the liquid solidifies into the Coulomb crystal at $T \leq T_{\text{m}}$. The melting temperature of a classical one–component plasma of ions corresponds to $\Gamma_{\text{m}} = 172$ (Nagara et al., 1987) and equals

$$T_{\text{m}} = \frac{Z^2 e^2}{a k_{\text{B}} \Gamma_{\text{m}}} \approx 1.32 \times 10^7 Z^{5/3} \left(\frac{\rho_{12}}{\mu_e} \right)^{1/3} \text{ K}. \quad (3)$$

Note that the crystallization of light nuclei (H, He) is additionally suppressed by strong zero-point vibrations (Mochkovitch and Hansen, 1979). The most bound is the body-centered-cubic

(bcc) crystal (see, e.g., Brush et al., 1966). The binding of the face-centered-cubic (fcc) crystal is weaker but very slightly. One cannot exclude that the fcc crystals appear in dense stellar matter along with the bcc ones (e.g., Baiko and Yakovlev, 1995). We will consider the temperature range of crystalline crust $T_U < T < T_m$, where $T_U \sim T_p Z^{1/3} e^2 / (\hbar v_F)$ is the temperature below which the Umklapp processes are frozen out (e.g., Raikh and Yakovlev, 1982), $T_p = \hbar \omega_p / k_B \approx 7.83 \times 10^9 \sqrt{Z \rho_{12} / (A \mu_e)}$ K is the ion plasma temperature, $\omega_p = \sqrt{4\pi Z^2 e^2 n_i / m_i}$ is the ion plasma frequency, and m_i is the ion mass. Note that the Debye temperature of a crystal is $T_D \approx 0.45 T_p$ (Carr, 1961). If $T \gtrsim T_U$ the electron–phonon scattering can be described using the approximation of almost free electrons. Then, at $Z \gg 1$, the main contribution into the scattering comes from the Umklapp processes (Yakovlev and Urpin, 1980, Raikh and Yakovlev, 1982).

For illustration, we will consider two models of matter in a NS crust: ground state (cold–catalyzed) matter and accreted matter. The effects of temperature onto the nuclear composition will be neglected which is justified as long as $T < 5 \times 10^9$ K (see Haensel et al., 1996). Both models assume that nuclei of one species are available in matter at any density (pressure). This leads to jumps of nuclear composition with increasing density (pressure).

The ground–state matter in the outer NS crust will be described using the data obtained by Haensel and Pichon (1994) from new laboratory measurements of nuclear masses with large neutron excess. For the inner crust, we will use the results of Negele and Vautherin (1973) derived on the basis of a modified Hartree–Fock method.

We will use the recent calculations of Haensel and Zhidunik (1990b), for describing accreted matter. The light elements are assumed to be burnt out in the outer layers of the NS crust while the nuclear composition in the deeper layers (we are interested in) is determined by a sequence of nuclear transmutations which occur in a sinking and compressing accretion matter and which depend neither on temperature nor on accretion rate.

The comparison of the ground–state and accreted matters is given, for instance, by Haensel and Zhidunik (1990a, b) or Haensel et al. (1996). At $\rho \gtrsim 10^9$ g cm $^{-3}$, the accreted matter is generally composed of lighter nuclei with lower Z . For instance, at $\rho = 4 \times 10^{12}$ g cm $^{-3}$ the accreted matter contains neutron–rich magnesium nuclei, $A = 44$, $Z = 12$ (Haensel and Zhidunik, 1990a, b), whereas the ground–state matter is composed of tin nuclei, $A = 159$, $Z = 50$ (Negele and Vautherin, 1973). The above difference is important for thermodynamic and kinetic properties of matter. For instance, the melting temperature (3) of the accreted matter at 10^{11} g cm $^{-3} \lesssim \rho \lesssim 10^{13}$ g cm $^{-3}$ is about 3 – 10 times lower than that of the ground–state matter (Figure 1).

3 General expressions

We can use the scheme of extended Brillouin zones and the free–electron approximation for describing the electron states. In this case, the Fermi surface and the electron dispersion relation are the same as for free electrons. This approximation is violated only in the narrow regions of momentum space near intersections of the electron Fermi surface with the Brillouin zone boundaries where the dispersion relation contains the energy gap. Note that the interzone electron transitions which accompany the neutrino–pair emission due to the Bragg diffraction (Section 1) occur just in these regions. The presence of the gap suppresses these transitions exponentially (Pethick and Thorsson, 1994).

A general expression for the neutrino energy loss rate Q due to the electron–phonon scattering of relativistic and degenerate electrons can be obtained using the standard formalism of the electron–phonon interaction (Ziman, 1960). In analogy with the results of Haensel et al. (1996), Q can be written as

$$Q = \frac{8\pi G_{\text{F}}^2 Z^2 e^4 C_{\pm}^2}{567\hbar^9 c^8} (k_{\text{B}}T)^6 n_{\text{i}} L \approx 3.229 \times 10^{11} \rho_{12} X_{\text{A}} \frac{Z^2}{A} T_8^6 L \text{ ergs s}^{-1} \text{ cm}^{-3}, \quad (4)$$

where $G_{\text{F}} = 1.436 \times 10^{-49}$ ergs cm³ is the Fermi weak–coupling constant, X_{A} is the mass fraction contained in nuclei, L is a dimensionless function of the parameters of stellar matter which has meaning of the Coulomb logarithm in the liquid phase. Furthermore, $C_{\pm}^2 = C_{\text{V}}^2 + C_{\text{A}}^2 + 2(C'_{\text{V}}^2 + C'_{\text{A}}^2)$, where C_{V} and C_{A} are the vector and axial–vector constants of weak interaction, respectively. We have $C_{\text{V}} = 2\sin^2\theta_{\text{W}} + 0.5$ and $C_{\text{A}} = 0.5$, for the emission of the electron neutrinos (charged + neutral currents); and $C'_{\text{V}} = 2\sin^2\theta_{\text{W}} - 0.5$ and $C'_{\text{A}} = -0.5$, for the emission of the muonic and tauonic neutrinos (neutral current only). In this case, θ_{W} is the Weinberg angle, $\sin^2\theta_{\text{W}} \simeq 0.23$. Numerical estimate of Q is obtained taking into account the contribution of the electron, muon and tau neutrinos which yields $C_{\pm}^2 \approx 1.675$.

The general expression for L in Equation (4) can be presented in the form

$$L = \frac{\alpha_0}{2tS^2} \int_S \int_S \frac{dS dS'}{q^2 |\epsilon(q)|^2} \left(1 + \frac{2y^2}{1-y^2} \ln y \right) e^{-2W(q)} \\ \times |f(q)|^2 \sum_s [\mathbf{q}\mathbf{e}_s(\mathbf{k})]^2 \frac{H(z)}{z^2}, \quad (5)$$

where

$$t = \frac{T}{T_{\text{p}}} = 0.0128 T_8 \left(\frac{A\mu_e}{Z\rho_{12}} \right)^{1/2}, \quad z \equiv z_s = \frac{\hbar\omega_s(\mathbf{k})}{k_{\text{B}}T}, \\ H(z) = \frac{63z}{16\pi^6} \int_0^\infty dw w^4 \left[\frac{w+z}{(1-e^{-z})(e^{w+z}-1)} + \frac{w-z}{(e^z-1)(e^{w-z}-1)} \right]. \quad (6)$$

In this case, $s=1, 2, 3$ enumerates three phonon modes in a Coulomb crystal. The integration in Equation (5) is carried out over possible momenta of electrons \mathbf{p} and \mathbf{p}' on the Fermi surface before and after scattering; $S = 4\pi p_{\text{F}}^2$ is the Fermi surface area. The quantity $\hbar\mathbf{q} = \mathbf{p} - \mathbf{p}'$ is an electron momentum transfer in a scattering event and $y = \hbar q/(2p_{\text{F}})$. Furthermore, \mathbf{k} , $\omega_s(\mathbf{k})$ and $\mathbf{e}_s(\mathbf{k})$ are, respectively, the wave vector, frequency and polarization unit vector of a phonon excited or absorbed by an electron: $\pm\mathbf{k} = \mathbf{q} - \mathbf{K}$, where \mathbf{K} is an inverse lattice vector chosen in such a way that \mathbf{k} belongs to the first Brillouin zone; the neutrino–pair momentum can be neglected here. The case of $\mathbf{k} = \mathbf{q}$ ($\mathbf{K}=0$) corresponds to a so called normal scattering process, while the case of $\mathbf{k} \neq \mathbf{q}$ ($\mathbf{K} \neq 0$) corresponds to an Umklapp process. The quantity $\epsilon(q)$ in Equation (5) is the longitudinal static dielectric function of the electron gas: it takes into account the electron screening of the Coulomb potential of a nucleus; $f(q)$ is the nuclear formfactor to allow for a finite nuclear size. Two terms under the integral in $H(z)$ describe the neutrino–pair radiation due to emission and absorption of phonons. The dimensionless integration variable is $w = \varepsilon_{\nu}/(k_{\text{B}}T)$, where ε_{ν} is the total energy of a neutrino–pair. Finally, $W(q)$ is the Debye–Waller factor. Baiko and Yakovlev (1995) fitted this factor for a Coulomb crystal (with a mean error of about 1%) by the expression $2W(q) = \alpha y^2$, where

$$\alpha = \alpha_0 \left(\frac{1}{2} u_{-1} e^{-9.100t} + t u_{-2} \right), \quad \alpha_0 = \frac{4m_e^2 c^2}{k_{\text{B}} T_{\text{p}} m_{\text{i}}} x^2 \approx 1.683 \sqrt{\frac{x}{AZ}}. \quad (7)$$

Here, $u_n = \langle (\omega/\omega_p)^n \rangle$ is a frequency moment of the phonon spectrum. Brackets mean averaging over phonon frequencies and polarizations:

$$\langle f_s(\mathbf{k}) \rangle = \frac{1}{3V_B} \sum_s \int_{V_B} d\mathbf{k} f_s(\mathbf{k}), \quad (8)$$

V_B is the Brillouin zone volume. One has $u_{-1}^{(bcc)} = 2.800$, $u_{-2}^{(bcc)} = 12.998$ for the bcc lattice (e.g., Mochkovitch and Hansen, 1979), and $u_{-1}^{(fcc)} = 4.03$, $u_{-2}^{(fcc)} = 28.8$ for the fcc one (e.g., Baiko and Yakovlev, 1995). According to Equation (5), the Debye–Waller factor suppresses the electron–phonon interaction at large momentum transfers q , and weakens the neutrino emission. The factor is important at large ion vibrations in the lattice — near the melting point (where the thermal vibrations are especially strong) and at high densities (where zero–point vibrations are huge). Under the conditions of study (Section 2) this factor is most significant.

In calculations based on Equation (5) we will use the static dielectric function of the degenerate relativistic electron gas $\epsilon(q)$ derived by Jancovici (1962). In our case, the electron screening is weak and has practically no effect on the results. Nevertheless we will take it into account.

We will use the nuclear formfactor appropriate for spherical nuclei with a uniform proton core:

$$f(q) = \frac{3}{(qr_c)^3} [\sin(qr_c) - qr_c \cos(qr_c)], \quad (9)$$

where, r_c is the core radius (which can be noticeably smaller than the total nucleus radius if the nucleus is neutron–rich). The formfactor suppresses the electron–phonon scattering at large momentum transfers q . One has $f(q) = 1$, for point–like nuclei.

It is convenient to fit $H(z)$ by an analytic function. One can easily see that $H(0) = 1$, and $H(z) = 21 z^7 e^{-z}/(160\pi^6)$ at $z \rightarrow \infty$. We have calculated $H(z)$ numerically for intermediate values of z . The calculated values and the asymptotes are reproduced (with the mean error of 1.7 %) by the fit

$$H(z) = \left(0.2968 + \sqrt{0.01633 z^2 + 0.7032^2}\right)^7 \exp\left(5.5032 - \sqrt{z^2 + 5.5032^2}\right). \quad (10)$$

4 Calculations and fitting of the results

Evaluation of L reduces to a 4-fold integration in Equation (5) over positions of electron momenta on the Fermi surface before and after scattering. For some parameters of stellar matter, the integration has been carried out numerically by the Monte Carlo method. We have used the code developed by Baiko and Yakovlev (1995) for calculating analogous integrals which determine the thermal and electric conductivities of electrons due to electron–phonon scattering. We have modified the code for calculating L . Typical calculation error for 10^6 Monte Carlo configurations (choices of positions of electron momenta on the Fermi surface before and after scattering) has been 6 % (at the 3σ level).

In order to simplify calculations and analyse the results, we have used also the simplified method of integration of the equations similar to (5), which was used earlier by Yakovlev and Urpin (1980), Raikh and Yakovlev (1982), Itoh et al. (1984b, 1993), and Baiko and Yakovlev (1995) in calculations of the thermal and electric conductivities. The method is based on the fact that the main contribution into the electron–phonon scattering comes from the Umklapp

processes. The Fermi surface is intersected by many boundaries of the Brillouin zones. Then, for the Umklapp processes, in Equation (5) one can approximately set

$$\sum_s [\mathbf{q}e_s(\mathbf{k})]^2 H(z)z^{-2} \approx q^2 t^2 G(t), \quad (11)$$

$$G(t) = t^{-2} \langle H(z)z^{-2} \rangle, \quad (12)$$

where brackets denote the averaging (8). As a result, from Equation (5) we obtain

$$L = \alpha_0 t G(t) P. \quad (13)$$

Here,

$$P = \int_{y_0}^1 y \, dy \frac{|f(q)|^2}{|\epsilon(q)|^2} \left(1 + \frac{2y^2}{1-y^2} \ln y \right) e^{-\alpha y^2}, \quad (14)$$

$y = \hbar q / (2p_F)$, and the lower integration limit $y_0 = \hbar q_0 / (2p_F) = (4Z)^{-2/3}$ is chosen in such a way to include the Umklapp processes but exclude the normal ones. The minimum momentum $q_0 = (6\pi^2 n_i)^{1/3}$ is set equal to the radius of the sphere whose volume equals the Brillouin zone volume.

Calculation of L from the approximate expression (13) reduces to determination of the two functions, G and P , that is much simpler than the exact Monte Carlo integration. Thus the calculations have been done mainly by the simplified method whose accuracy has been controlled by the Monte Carlo runs at some parameter values. In all the cases, the results have coincided, within the Monte Carlo error bars.

The function G depends on the dimensionless temperature t , given by Equation (6), and on the lattice type. If $t \gg 1$, from Equations (6) and (12) we obtain the asymptote $G(t) = u_{-2}$, where u_{-2} is a frequency moment of the phonon spectrum (Section 3). When $t \rightarrow 0$ we have $G(t) \sim t$. We have calculated $G(t)$ from Equation (12) for the bcc and fcc lattices using the approximate but highly accurate method proposed by Mochkovitch and Hansen (1979) for averaging the expressions similar to (8) over the Brillouin zone. The results can be fitted (with about 1.5 % mean error) by the function

$$G(t) = \frac{u_{-2}t}{\sqrt{a_0^2 + t^2}} + \frac{b_1 t^3}{(b_2 + t^2)^2}, \quad (15)$$

where $a_0^{(bcc)} = 0.06423$, $b_1^{(bcc)} = 0.1151$, $b_2^{(bcc)} = 5.92 \times 10^{-4}$; $a_0^{(fcc)} = 0.001479$, $b_1^{(fcc)} = 0.2381$, $b_2^{(fcc)} = 5.161 \times 10^{-4}$. This expression reproduces also the above asymptotes.

The function P is given by a simple one-dimensional integral, which is insensitive to the crystal type but depends on three parameters: atomic number Z (through the lower integration limit, y_0), the Debye–Waller parameter $\alpha = \alpha(t)$ (see Equation (7)), and the parameter $\eta = r_c/a$ which accounts for the finite size of atomic nuclei in the nuclear formfactor (9) (a is given by Equation (3)). We have evaluated P from Equation (14) at $Z = 20, 40, 60$, $\alpha = 0.04, 0.12, 0.4, 1.2, 4, 12$ and $\eta = 0, 0.10, 0.2, 0.3, 0.4$. Analysing the parameters of matter in a NS crust at $10^6 \text{ g cm}^{-3} \lesssim \rho \lesssim 10^{14} \text{ g cm}^{-3}$ (Section 2), one can show that the selected values cover all the domain of possible parameter values. The results are fitted by the expression

$$P(Z, \alpha, \eta) = \frac{F_0}{2} \left[1 + \frac{(18\pi Z)^{2/3} F_1}{5N F_0} \eta^2 \right]^{-N}, \quad (16)$$

where $2p_{\text{F}}r_c/\hbar = (18\pi Z)^{1/3}\eta$, $N = 3.781 - 0.02322 Z$, and the functions F_0 and F_1 are given by

$$F_0 = \frac{1}{\alpha} (e^{-u} - e^{-\alpha}) - 0.6449 \frac{e^{-0.3462\alpha}}{1 + \alpha} - \frac{s^2}{2} [\ln(s) - 0.5] e^{-\alpha} + \frac{\alpha(1+u)}{(1+\alpha)^3} \left[\ln\left(\frac{1+u}{1+\alpha}\right) - 0.4230 \right] e^{-u}, \quad (17)$$

$$F_1 = \frac{1}{\alpha^2} [(1+u)e^{-u} - (1+\alpha)e^{-\alpha}] - 0.3949 \frac{e^{-0.4726\alpha}}{(1.5+\alpha)^{3/4}} - \frac{s^3}{3} [\ln(s) - 5.213] e^{-\alpha} + \frac{\alpha(2+4u+u^2)}{(1.5+\alpha)^4} \left[\ln\left(\frac{1+u}{1.5+\alpha}\right) - 0.1 \right] e^{-u}. \quad (18)$$

Here, $s = (4Z)^{-2/3} + 0.00563$, $u = s\alpha$. The mean error of the fit (16) is 1.3 %, and the maximum error of 3.9 % takes place at $t=0.12$, $Z=60$, $\eta=0.3$.

Note a simple asymptote $L \approx 0.5$ which is valid in the limiting case when $t \gg 1$, $\alpha \gg 1$ and $\alpha y_0^2 \ll 1$. However this asymptote cannot be actually realized in NS matter for the conditions of study (Section 2). In the opposite case, when $t \ll 1$, we obtain $L = \alpha_0 t^2 u_{-2} P / a_0$, where P should be calculated at $\alpha = 0.5\alpha_0 u_{-1}$ (see Equation (7)).

5 Discussion

Equations (4), (13), (15) and (16) allow us to evaluate easily the neutrino energy loss rate Q due to electron–phonon scattering for any model of stellar matter in the parameter range of study (Section 2).

Figures 2 – 4 display L as a function of the dimensionless temperature t . The maximum values of t correspond to the melting temperature (3). Following Itoh et al. (1984a), the proton core radius r_c in the nuclear formfactor (9) has been taken as: $r_c = 1.15A^{1/3}$ fm at $\rho < 4 \times 10^{11}$ g cm $^{-3}$; and $r_c = 1.83Z^{1/3}$ fm at higher ρ . If $\rho \lesssim 10^{11}$ g cm $^{-3}$ the nuclear size effect is unimportant and one can set $\eta = 0$.

Figure 2 corresponds to the ground–state matter (Section 2) at $\rho = 4 \times 10^{12}$ g cm $^{-3}$ ($A = 159$, $Z = 50$, Negele and Vautherin, 1973). The nuclear size effect is seen to decrease L and Q by (20–30) %. According to Equations (9) and (14), the nuclear formfactor decreases the integrand at large $y \approx 1$ (i.e., at large–angle scattering), and the effect is more pronounced with increasing η . However the integrand is already small at these y due to the Debye–Waller factor (which reduces the scattering with large momentum transfers) and due to the factor $[1+(2y^2/(1-y^2))\ln(y)]$. The latter factor describes suppression of backward scattering of relativistic electrons (see Haensel et al., 1996) and vanishes at $y = 1$. This explains weak dependence of L on η .

The temperature dependence of L in the bcc and fcc crystals is similar. The $L(t)$ curve for the bcc crystal has formally the maximum, just as the bcc curve, but this happens at higher t , above the melting temperature. The maximum of $L(t)$ for the fcc crystal is shifted to lower t (and seen in Figure 2) owing to a softer phonon spectrum (see Baiko and Yakovlev, 1995).

Let us emphasize that the neutrino emission due to the electron–phonon scattering in the bcc crystal was calculated earlier by Itoh et al. (1984a). These results are also included in the new review article of Itoh et al. (1996). The authors calculated the function F_{phonon} related to our function L as $F_{\text{phonon}} = 2L/3$. The calculations of F_{phonon} were carried out for the nuclei of ^4He , ^{12}C , ^{16}O , ^{20}Ne , ^{24}Mg , ^{28}Si , ^{32}S , ^{40}Ca , ^{56}Fe at 10^4 g cm $^{-3} \lesssim \rho \lesssim 10^{12}$ g cm $^{-3}$ and also for

the ground-state matter at $10^4 \text{ g cm}^{-3} \lesssim \rho \lesssim 10^{14} \text{ g cm}^{-3}$. The results were fitted (Itoh et al. 1984a, 1996) by very complicated expressions which require large tables of fit parameters. Our fits (Section 4) are much simpler and valid for any nuclear composition. For comparison, Figure 2 presents the temperature dependence of $L(t)$ (long dashes) for the bcc crystal derived using the fits of Itoh et al. (1984a, 1996). The results are somewhat different from those obtained in the present article. The difference (which is sometimes rather large) takes place also for other values of ρ , T , and for other elements (Figures 3 and 4).

This difference is likely to come from not too accurate fits of Itoh et al. (1984a, 1996). In order to confirm this statement let us compare the equations of Itoh et al. (1984a) and the equations of the present article. Itoh et al. (1984a) used another method of calculation taken from the earlier article of Flowers (1973). For comparison, we express the integral (14) in Equation (13) as a three-dimensional integral over electron momentum transfers $d\mathbf{q}$. Flowers (1973) and Itoh et al. (1984a) replaced the latter integration by summation over possible inverse lattice cells where \mathbf{q} could appear. The integration over any cell of the sum was done by replacing $\mathbf{q} = \mathbf{K}$. In addition, just as in the present article, the normal scattering processes were neglected, i.e., the contribution from the central cell was excluded. For comparison, we have also calculated L by the same method of summation over inverse lattice cells. The results (short-dashed curves in Figures 3 and 4) are in good agreement with our original results (for chosen nuclei and densities) but differ from those given by the fits of Itoh et al. (1984a, 1986) by a factor of several.

Figure 5 demonstrates the neutrino energy loss rate $E = Q/\rho$ per unit mass ($\text{ergs s}^{-1} \text{ g}^{-1}$) as a function of density at several values of temperature for the ground-state and accretion matters (Section 2). Note that the selfconsistent models of accreted matter correspond to temperatures $T \sim 10^8 \text{ K}$ (Miralda-Escudé et al., 1990). We have extended the accretion model to higher T for illustrative purpose, to demonstrate the effect of variation of nuclear composition onto the neutrino emission rate. For the displayed parameters, the matter can be either in the liquid or in the solid phase. The emissivity E in the solid phase has been calculated using the expressions of Section 4 (for bcc crystals). In the liquid phase, we have used the formulae of Haensel et al. (1996). Nuclear composition varies at certain values of density as described in Section 2 (Figure 1). In addition, there occur liquid-solid phase transitions at certain ρ which are easily deduced from Figure 1. For all T displayed in Figure 5, the matter of sufficiently high density becomes solid. With decreasing T , the crystallization boundary shifts towards lower densities. The accreted matter solidifies at somewhat higher ρ since it contains nuclei with lower Z . In addition, if $T = 8 \times 10^8 \text{ K}$ and ρ increases in the accreted matter and becomes higher than $\rho \gtrsim 10^{11} \text{ g cm}^{-3}$ there occurs a series of transitions from liquid into solid and back. This effect is associated with strongly nonmonotonic melting temperature due to rapid changes of Z (Figure 1).

According to Equation (4), the dependence of the neutrino energy loss rate E on ρ and T is determined by the factor $(X_A Z^2/A) T_8^6 L$. If $X_A Z^2/A$ and L were fixed, the emissivity E would be displayed by horizontal lines in Figure 5. Actually, however, E varies with ρ . The curves are seen to suffer jumps associated with changes of the nuclear composition and crystallization. The jumps due to variations of the nuclear composition are much weaker. In a crystallization point, the function L and the emissivity E decrease steeply by a factor of 1.5–3 but the general character of the density dependence of E in the liquid phase and just after the crystallization is the same. This is because the neutrino-pair bremsstrahlung by electrons due to the Coulomb scattering in a liquid is similar to that due to the high-temperature electron-phonon scattering ($T \gtrsim T_p$). Indeed, the function L is rather smooth either in the liquid (Haensel et al., 1996), or

in the high-temperature crystal, and it behaves as $E \propto (X_A Z^2/A)T^6$, in the first approximation. The crystallization jump of E can be somewhat smoothed if we additionally take into account the exponentially suppressed static lattice contribution (Pethick and Thorsson, 1994). However, our preliminary estimates based on the approximate expressions given by Pethick and Thorsson (1994) and Itoh et al. (1996) show that the smoothing is not significant.

With increasing ρ inside the crystalline phase (at a fixed temperature T), the ratio $t = T/T_p$ generally decreases, and the low-temperature phonon scattering becomes important. In this regime, according to the results of Section 4, the function $L = \alpha_0 t^2 u_{-2} P/a_0$, and P depends weakly on the parameters of stellar matter. Then one has a strong ($\sim t^2$) suppression of the neutrino generation. The generation rate becomes a sharper function of T and depends explicitly on ρ . In the first approximation, $E \propto T^8 (A/Z)^{1/3} X_A^{1/6} \rho^{-5/6}$. The suppression leads to a noticeable decrease of E with ρ (Figure 5). The dependence of E on nuclear composition becomes much weaker, than in the liquid or high-temperature crystal. This explains increasing similarity of the emissivities $E(\rho)$ for the ground-state and accreted matters in Figure 5 with decreasing T and/or increasing ρ . At $T \lesssim 5 \times 10^8$ K the difference of the emissivities becomes negligibly small.

As follows from Figure 5, the neutrino emissivity E is much more sensitive to the state of matter (liquid or crystal) than to nuclear composition (accreted or ground-state matter). For instance, it is easy to calculate the emissivity E for matter composed of iron nuclei ^{56}Fe and show that it differs slightly from the curves presented in Figure 5.

6 Conclusions

We have calculated (Section 3) the neutrino energy loss rate due to electron-phonon scattering in the Coulomb bcc and fcc crystals of spherical atomic nuclei at densities $10^6 \text{ g cm}^{-3} \ll \rho \lesssim 10^{14} \text{ g cm}^{-3}$ and temperatures $T_U \lesssim T \leq T_m$ in matter of arbitrary nuclear composition (Section 2). The results are fitted by simple expressions (Section 4). Combined with the results of Haensel et al. (1996), which describe the neutrino emission due to the bremsstrahlung in the liquid phase ($T_m < T \lesssim T_F$), the equations obtained allow one to evaluate easily the neutrino energy loss rate due to the bremsstrahlung process in the wide temperature range $T_U \lesssim T \lesssim T_F$, most important for applications. The main properties of the neutrino energy losses are analysed in Section 5 for two models of matter in a NS core (described in Section 2): ground-state and accreted matter. Note that at very low temperature ($T \ll T_m$) the neutrino emission due to the electron-phonon scattering may appear so weak that another neutrino generation mechanism becomes dominant — the Coulomb scattering of electrons by charged impurities. The corresponding neutrino energy loss rate can be easily calculated, for instance, from the results of Haensel et al. (1996). However the neutrino emission at these low temperatures is expected to be too weak to be of practical interest.

The results of the present article can be useful for numerical modelling of various processes associated with thermal evolution of NSs. First of all, we mean cooling of young NSs (of age $\lesssim (1 - 10^3)$ yrs), where thermal relaxation is not yet achieved (Lattimer et al., 1994). The relaxation is accompanied by a cooling wave which goes from the stellar interior to the surface. Corresponding variations of the surface temperature are, in principle, observable. The dynamics of thermal relaxation is quite sensitive to the properties of matter in the NS crust, especially to nuclear composition and neutrino energy losses.

The authors are grateful to C. Pethick and V. Thorsson for very useful discussions, to D.A. Baiko for assistance in Monte Carlo calculations, and to N. Itoh for presenting the review article of Itoh et al. (1996) prior to publication. This work was partially supported by the Russian Basic Research Foundation (grant 93-02-2916), the Soros Foundation (grant R6A-003), and INTAS (grant 94-3834).

References

- Baiko, D.A. and Yakovlev, D.G., *Pisma Astron. Zh. (Astron. Lett.)*, 1995, v. 21, p. 784.
- Brush, S.G., Sahlin, H.L., Teller, E. J., *Chem. Phys.*, 1966, v. 45, p. 2102.
- Carr, W.J., *Phys. Rev.*, 1961, v. 122, p. 1437.
- Flowers, E., *Astrophys. J.*, 1973, v. 180, p. 911.
- Haensel, P. and Zdunik, J.L., *Astron. Astrophys.*, 1990a, v. 227, p. 431.
- Haensel, P. and Zdunik, J.L., *Astron. Astrophys.*, 1990b, v. 229, p. 117.
- Haensel, P. and Pichon, D., *Astron. Astrophys.*, 1994, v. 283, p. 313.
- Haensel, P., Kaminker, A.D., Yakovlev, D.G., *Astron. Astrophys.*, 1996 (in press).
- Ito, N. and Kohyama, Y., *Astrophys. J.*, 1983, v. 275, p. 858.
- Itoh, N., Kohyama, Y., Matsumoto, N., Seki, M., *Astrophys. J.*, 1984a, v. 285, p. 304.
- Itoh, N., Kohyama, Y., Matsumoto, N., Seki, M., *Astrophys. J.*, 1984b, v. 285, p. 758; erratum: v. 404, p. 418.
- Itoh, N., Adachi, T., Nakagawa, M., Kohyama, Y., Munakata, H., *Astrophys. J.*, 1989, v. 339, p. 354; erratum: 1990, v. 360, p. 741.
- Itoh, N., Hayashi, H., Kohyama, Y., *Astrophys. J.*, 1993, v. 418, p. 405.
- Itoh, N., Hayashi, H., Nishikawa, A., Kohyama, Y., *Astrophys. J. Suppl.*, 1996 (in press).
- Jancovici, B., *Nuovo Cimento*, 1962, v. 25, p. 428.
- Lattimer, J.M., Van Riper, K., Prakash, M., Prakash, M., *Astrophys. J.*, 1994, v. 425, p. 802.
- Lorenz, C.P., Ravenhall, D.G., Pethick, C.J., *Phys. Rev. Lett.*, 1993, v. 70, p. 379.
- Miralda-Escudé, J., Haensel, P., Paczyński, B., *Astrophys. J.*, 1990, v. 362, p. 572.
- Mochkovitch, R. and Hansen, J.-P., *Phys. Lett.*, 1979, v. A73, p. 35.
- Nagara, H., Nagata, Y., Nakamura, T., *Phys. Rev.*, 1987, v. A36, p. 1859.
- Negele, J.W. and Vautherin, D., *Nucl. Phys.*, 1973, v. A207, p. 298.
- Pethick, C.J. and Ravenhall, D.G., *Ann. Rev. Nucl. Particle Sci.*, 1995, v. 45, p. 429.
- Pethick, C.J. and Thorsson, V., *Phys. Rev. Lett.*, 1994, v. 72, p. 1964.
- Raikh, M.E. and Yakovlev, D.G., *Astrophys. Space Sci.*, 1982, v. 87, p. 193.
- Yakovlev, D.G. and Urpin, V.A., *Sov. Astron. Lett.*, 1980, v. 24, p. 303.
- Ziman, J.M., *Electrons and Phonons*, Oxford University Press: Oxford, 1960.

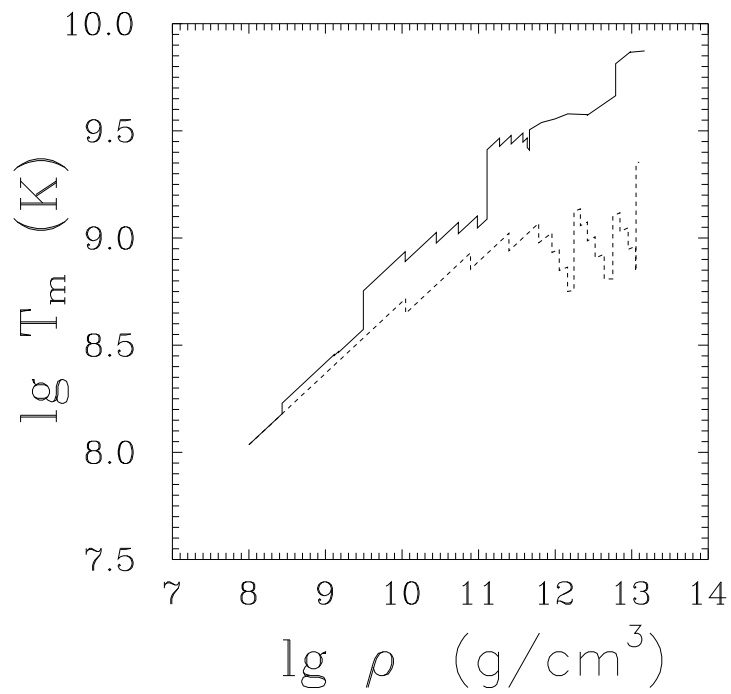


Figure 1: Melting temperatures of the ground-state (solid line) and accreted (dash line) matter.

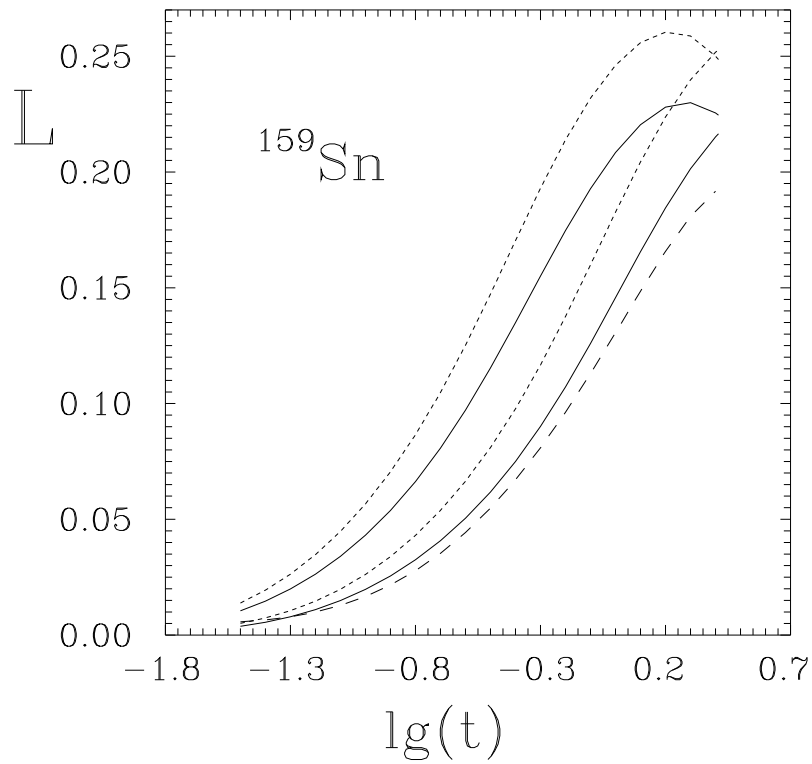


Figure 2: Quantity L versus $t = T/T_p$ for the bcc (lower curves) and fcc (upper curves) crystals composed of ^{159}Sn nuclei at density $\rho = 4 \times 10^{12} \text{ g cm}^{-3}$ with account for the finite nuclear size ($\eta = 0.15$, solid lines) and for point-like nuclei ($\eta = 0$, short dashes). Long dashes — fits of Itoh et al. (1984a).

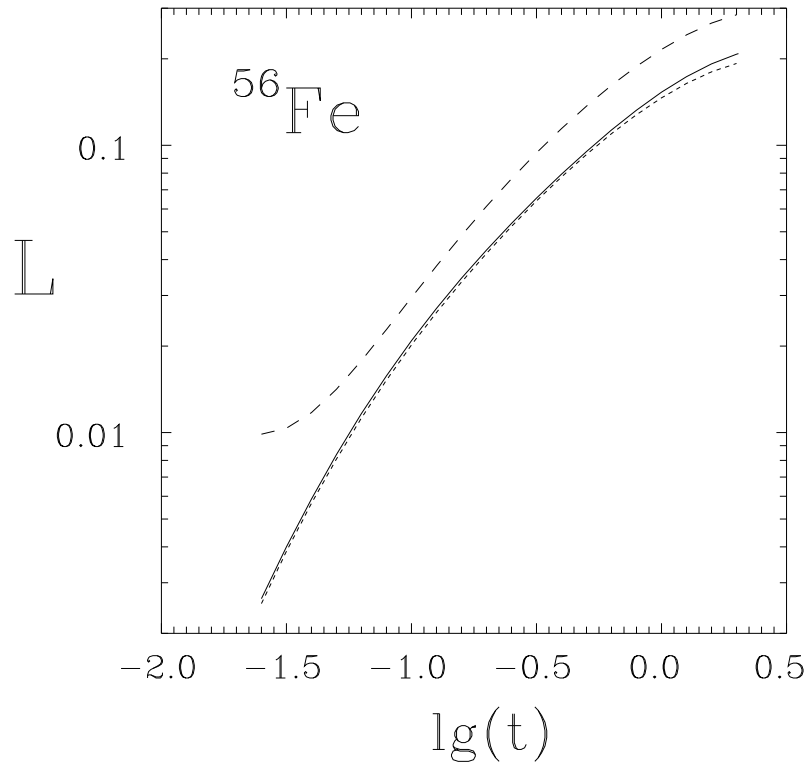


Figure 3: Quantity L versus t for the bcc crystal composed of ^{56}Fe nuclei at $\rho = 10^9 \text{ g cm}^{-3}$. Solid line — present calculation, long dashes — fit of Itoh et al. (1984a, 1996), short dashes — present calculation using the method of Itoh et al. (1984a).

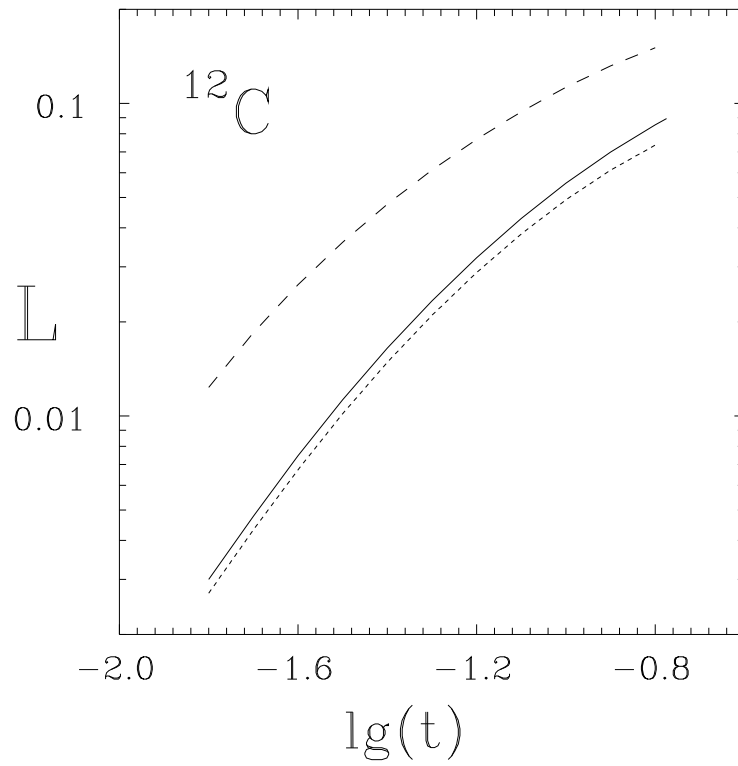


Figure 4: Same as in Figure 3, but for the crystal composed of ^{12}C .

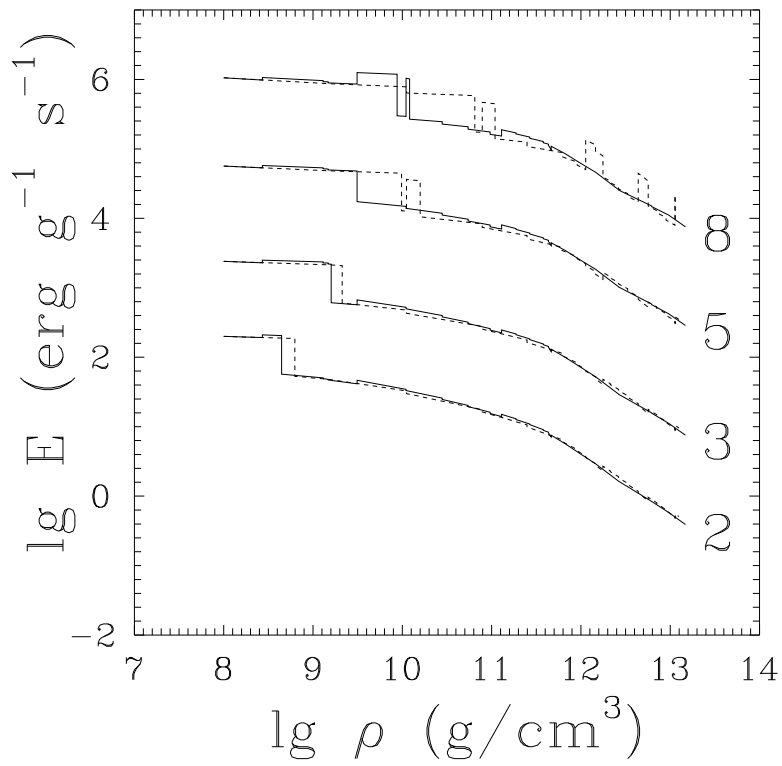


Figure 5: Neutrino energy loss rate due to the bremsstrahlung produced by electron-nucleus ($T > T_m$) or electron-phonon scattering ($T < T_m$) versus density for the ground-state (solid lines) and accreted (dash lines) matters at several values of T (values of T_8 are shown near the curves).